ACS Photonics

pubs.acs.org/journal/apchd5

Letter

Terahertz Spectroscopy of Gas Mixtures with Dual Quantum Cascade Laser Frequency Combs

Lukasz A. Sterczewski,[#] Jonas Westberg,[#] Yang Yang, David Burghoff, John Reno, Qing Hu, and Gerard Wysocki*

Cite This: *ACS Photonics* 2020, 7, 1082−1087

Read Online

ACCESS | Metrics & More | Article Recommendations

ABSTRACT: Terahertz laser frequency combs based on quantum cascade lasers provide coherent, broadband, electrically pumped, THz radiation sources for use in future spectroscopic applications. Here, we explore the feasibility of such lasers in a dual-comb spectroscopy configuration for the detection of multiple molecular samples in the gas phase. The lasers span approximately 180 GHz of optical bandwidth, centered at 3.4 THz, with submilliwatt total optical power. One of the main advantages of dual-comb spectroscopy is its high speed, which opens up the possibility for direct observations of chemical reaction dynamics in the terahertz spectral region. As a proof-of-concept, we recorded continuously evolving spectra from gas mixtures with 1 ms temporal resolution.

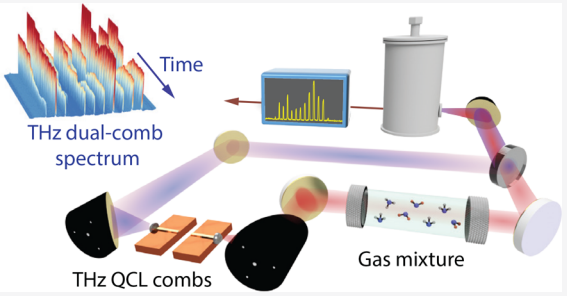

KEYWORDS: *terahertz, quantum cascade laser, frequency comb, dual-comb spectroscopy, multispecies, real-time*

For a long time, the terahertz part of the electromagnetic spectrum (0.1−20 THz) was experimentally inaccessible since it was too high in frequency for electronic circuitry and too low in frequency for coherent optical sources. However, recent advances in the generation of THz radiation primarily provided by the developments of photoconductive antennas,[1] femtosecond fiber lasers,[2] and optically pumped gas-phase molecular lasers[3,4] have resulted in a significant increase of research activity in the field of THz spectroscopy over the past decade. Greatly desired for this application are chip-scale electrically pumped quantum cascade laser (QCL) sources. Since their inception[5] and first demonstration in the far-infrared,[6] these sources have been successfully used as local oscillators for astronomy heterodyne receivers[7] or in metrological-grade spectrometers disciplined by atomic frequency standards.[8] Terahertz QC vertical-external-cavity surface-emitting lasers (VECSELs) offer now a nearly-Gaussian beam pattern, without the divergence and aberrations typical for edge-emitting lasers.[9] Also, by exploiting difference frequency generation (DFG) in mid-infrared QCLs, cryogenic temperatures are no longer a prerequisite for the operation of chip-scale THz sources. Room-temperature Cherenkov-scheme THz generation with broad tunability[10] promises proliferation of this technology on a larger scale.

Despite these advances, the field of THz spectroscopy is predominantly occupied by THz time-domain spectroscopy (TDS) with commercially available turn-key systems that provide reliable spectral coverage over a few THz. However, just like THz spectrometers based on the Fourier transform spectroscopy technique, these instruments often require an optical delay line with mechanically moving parts, which make them inherently slow, with spectral acquisition times in the order of seconds or longer.

Multiheterodyne spectroscopy or dual-comb spectroscopy (DCS) using QCL optical frequency combs (OFCs) is an interesting alternative that has proven to be viable in the mid-infrared spectral region, where broadband spectroscopy with high temporal resolution has been repeatedly demonstrated.[11,12] These all-solid-state semiconductor-based spectrometers do not require moving parts and can record spectra spanning several hundreds of GHz in just a few microseconds. Furthermore, the possibility of complete integration into a small package[13] makes them particularly intriguing for in situ applications in industry and consumer products.

The recent demonstrations of THz frequency combs[14,15] and proof-of-concept spectroscopy results obtained with a GaAs etalon,[16,17] as well as solids,[18] indicate the potential of extending this technology to perform spectroscopy of gases in the THz region. This work aims to further establish the

Received: December 12, 2019
Published: April 15, 2020

https://dx.doi.org/10.1021/acsphotonics.9b01758
ACS Photonics 2020, 7, 1082−1087

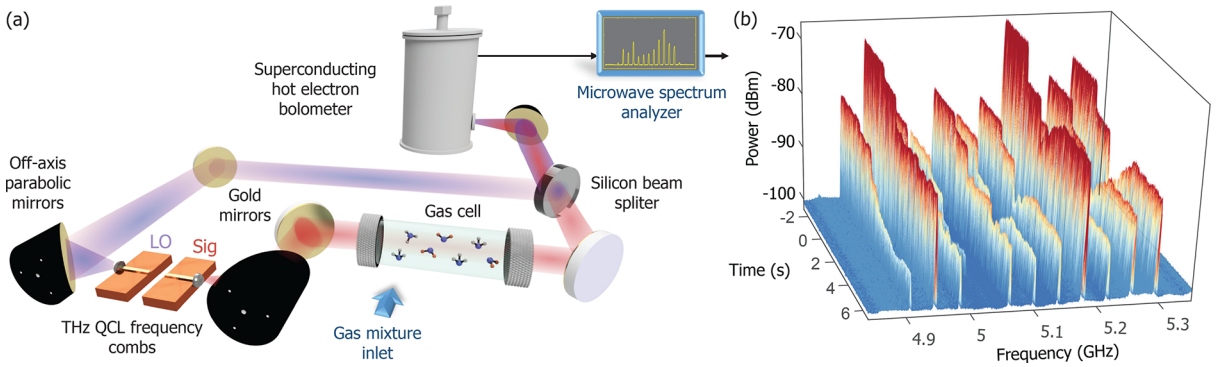

Figure 1. (a) Dual-comb spectroscopic system. Two free-running THz-QCL OFCs mounted antiparallel in a pulsed tube cryostat emit light centered at ∼3.4 THz, collected using external off-axis parabolic mirrors. Only the signal (Sig) OFC interrogates the gas absorption cell. The transmitted light is combined with the local oscillator (LO) comb on a silicon beam splitter and is next beaten on a GHz-bandwidth hot electron bolometer. A microwave spectrum analyzer records data in real time, without the need for computational coherent averaging or active feedback loop stabilization; (b) 9 s of THz-DCS data recorded with the microwave spectrum analyzers with 1 ms temporal resolution (9000 spectra). Each 1 ms frame corresponds to 39000 quasi-coherently averaged interferograms with a fundamental refresh rate defined by the spacing of the radio frequency comb equal to Δf_{rep} = 39 MHz.

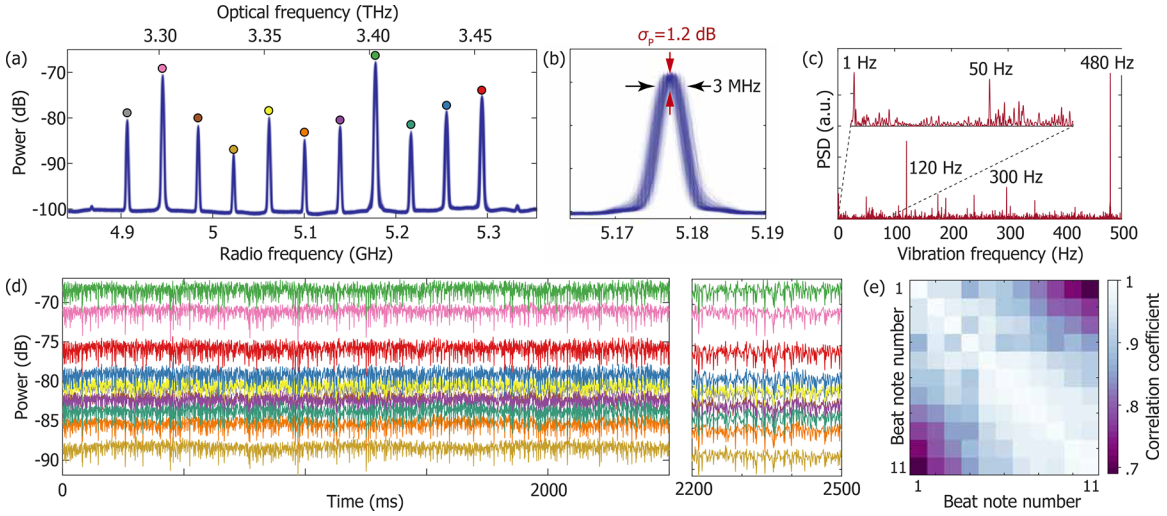

Figure 2. (a) Stacked 1000 rf dual-comb spectra measured in 1 ms each with the spectrum analyzer under free-running operation of the system. Due to cryostat vibrations, the beat notes jitter in amplitude and frequency, albeit even over such extended time scales they do not drift by more than a megahertz. Eleven beat notes are used for spectroscopy marked with colored dots; (b) Zoom on the most intensive beat note. The 3 dB line width is lower than 3 MHz, while the peak amplitude fluctuates from shot to shot by 1.2 dB (standard deviation); (c) Fourier analysis of the most intensive peak amplitude showing the dominant oscillation frequency at 480 Hz, which is the eighth harmonic of the AC mains driving the cryostat motor. Additionally, strong resonances occur at ∼300 Hz, 120 Hz, and the fundamental operation frequency of the cryocooler of ∼1 Hz; (d) Time series of all the 11 beat notes' rf powers used for the reference measurement showing high visual similarity. The right panel zooms over 300 ms, illustrating the synchronicity of amplitude fluctuations; (e) Mutual correlation analysis of beat note amplitudes. The mean pairwise correlation coefficient r_{ij} ($i, j \in \{1\cdots11\}$ and $i \neq j$) is 90.4%, while the maximum is 98.7%. Amplitude noise is highly correlated in our system.

feasibility of high temporal resolution THz spectroscopy using QCL OFCs by presenting the first QCL-based THz-DCS measurements of gas-phase molecular samples with millisecond time-resolution.

The experimental setup shown in Figure 1a is similar as reported in our earlier publications.[16,18] Two THz-QCL OFCs emitting light centered around 3.4 THz are mounted on a coldfinger and housed in a cryostat with a temperature of 25 K, maintained by a closed cycle cryocooler. A cartridge heater is used to actively stabilize the temperature of the coldfinger. The temperature is chosen to allow for good spectral overlap of the two combs while simultaneously ensuring low phase-noise operation. In addition, the laser injection currents are individually controlled to allow for fine-tuning of the laser frequencies. This also provides a means to individually adjust the repetition rates of the two combs. After collimation, the estimated optical power per tooth in each comb is ∼10 μW. Only one of the combs, here labeled as signal (Sig), interrogates the sample gas mixture, which is housed in a homemade 14 cm long stainless steel absorption cell with polymethylpentene (TPX) windows. After propagating through the absorbing species, the signal comb is combined with the local oscillator comb (LO) on a silicon beam splitter and guided to a superconducting NbN hot-electron bolometer (HEB) for multiheterodyne down-conversion of the THz spectrum to the radio frequency (rf) domain. The entire system is enclosed in an acrylic chamber purged with dry gaseous nitrogen to suppress the absorption of atmospheric humidity on the THz spectrum. Due to a mismatch in the repetition rates of the combs (16.988 and 17.027 GHz for the

https://dx.doi.org/10.1021/acsphotonics.9b01758
ACS Photonics 2020, 7, 1082−1087

Sig and LO comb, respectively), the down-converted comb in the rf has a frequency separation of Δf_{rep} = 39 MHz with ∼500 MHz of electrical bandwidth, which corresponds to ∼180 GHz of optical spectral coverage at 3.4 THz. The resulting microwave spectrum is recorded with a real-time spectrum analyzer (FSW-43, Rohde & Schwarz) with an acquisition time of 1 ms per spectra, as visualized in Figure 1b using a waterfall representation of the recorded short-term amplitude spectrum (spectrogram). The down-converted THz spectrum shows characteristic beat note amplitude attenuations induced by wavelength-dependent changes in the transmission through the sample cell when different gas mixtures are introduced.

Compared to earlier preliminary dual-comb experiments using THz-QCL combs,[16] our system shows improved robustness against optical feedback due to the introduction of a polyethylene (PE) spacer between the laser output facet and the silicon collimation lens, which provides an additional low refractive index layer. Since the PE layer effectively increases reflection at the output facet of the laser compared to the case when the silicon lens is directly attached to the output facet, it makes the laser less sensitive to unwanted optical feedback. In addition, mechanical vibrations are reduced using a system of copper braids and rubber dampeners to mechanically decouple the cryopump from the sample compartment (an option available on the SRDK-408 Cold-Edge cryocooler system). These improvements enable a completely free-running system without hardware phase-locked loops[19] for rf frequency stabilization or digital postcorrection algorithms for recovering the comb nature of the dual-comb signals.[20,21] The short-term coherence between the sources was sufficient to permit power spectrum averaging of the data within a 1.2 MHz resolution bandwidth, which additionally reduced the amount of stored data for prolonged (dozen of seconds) acquisitions. Figure 2a plots the persistence spectrum of a thousand 1 ms free-running spectra. Upon close examination, mechanical vibrations are not completely suppressed despite elaborate dampening mechanisms in the cryostat design. A zoom of the strongest beat note shown in Figure 2b reveals maximum fluctuations in frequency of ∼3 MHz (3 dB line width) over 1 s, while the standard deviation of the peak amplitude is 1.2 dB. This value is surprisingly high for the relatively long 1 ms acquisition time of each spectral frame in the MH spectrum and, yet, can be attributed to vibration noise affecting the combs. The (vibration) frequency spectrum of the quasi-instantaneous amplitude of the beat note is shown in Figure 2c. In addition to the fundamental cryostat pump frequency of ∼1 Hz, we observe a dominant contribution of even harmonics of 60 Hz known to appear in resonant mechanical systems. Also, the appearance of broader resonant features close to typical eigenfrequencies of the inner shield and the vacuum chamber of the cryostat (i.e., 50 Hz) suggest a mechanical origin.[22−24]

An analysis of all the beat note amplitudes in the system, retrieved using a quadratic peak interpolation algorithm,[26] shows highly correlated fluctuations. The transient dips in amplitude shown in Figure 2d clearly show that the cryostat pump-related slowly varying components appear at the same instances of time for all beat notes. The pairwise correlation coefficient map computed from the amplitude data set in panel (d) plotted in Figure 2e has a mean value (excluding the diagonal) of 90.4% and a maximum of 98.7%, which indicates strong correlation. In principle, the fluctuations of individual modes could be suppressed by the use of a reference detector, and the high correlation between the beat notes could allow a simpler amplitude suppression scheme using a slow THz power detector rather than a costly HEB. However, in this study, amplitude noise was suppressed through ordinary extended time-scale averaging.

Our proof-of-concept multispecies spectroscopic detection experiment was conducted in four phases, visualized by the background colors of the time-resolved dual-comb absorbance spectra in Figure 3. In each phase, we measured the final cell

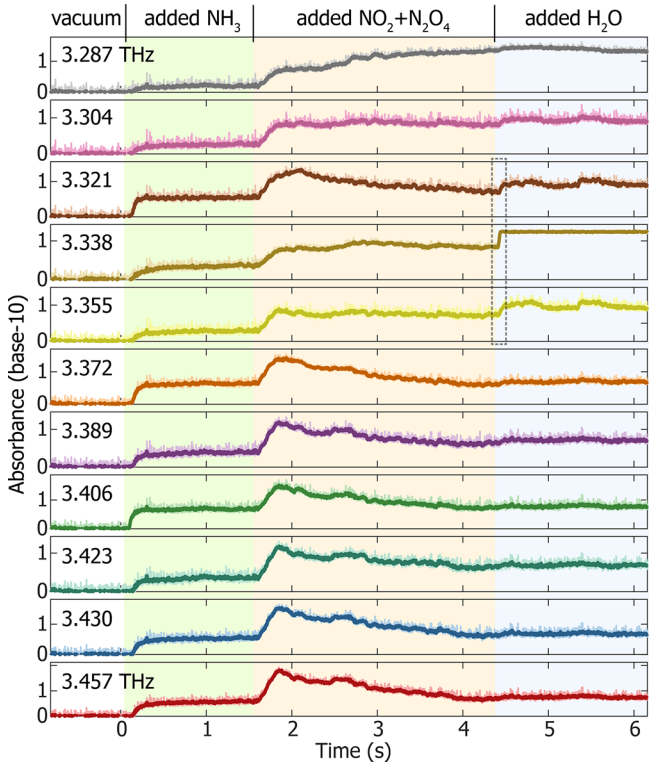

Figure 3. Time-resolved decadic (base-10) absorbance retrieved from the dual-comb spectrogram at the four phases of the experiment. Bold lines are 10-point moving averages.

pressure with a gauge to validate our spectroscopic model. In the first phase, the absorption cell was held under vacuum to obtain a zero-gas background spectrum used for calibration. Next, at time t = 0 s, anhydrous ammonia (NH_3) was introduced to the cell up to a total pressure of 200 Torr, which is accompanied by a step in absorbance (phase 2). In phase 3, starting at t = 1.6 s, nitrogen dioxide (NO_2), which exists in chemical equilibrium with dinitrogen tetroxide (N_2O_4), was added to the gas mixture. At lower temperatures, the formation of N_2O_4 is a preferred process, whereas at higher temperatures, formation of nitrogen dioxide predominates. A pressurized NO_2 cylinder is used to deliver the gas to the system. When the gas expands into the measurement gas cell, it rapidly lowers its temperature, thus, favoring the formation of solid and gaseous N_2O_4. The latter has shown to exhibit intensive absorption peaks at ∼113 cm^{-1} (3.39 THz)[27] with an unchanged molecular structure in the liquid, gaseous, and solid state.[28] Thus, the sudden increase of the absorption at ∼3.40 THz and its slow decay over several seconds is consistent with the formation of N_2O_4 by means of dimerization, followed by a slow transition to NO_2, when the system again reaches thermal equilibrium. The last phase starting at t = 4.4 s corresponds to

https://dx.doi.org/10.1021/acsphotonics.9b01758
ACS Photonics 2020, 7, 1082−1087

a sudden opening of the purged measurement chamber, which allowed atmospheric air (10% relative humidity) to leak into the system and thus cause severe water absorption at ~3.34 THz. The optical frequencies were retrieved from a multipoint spectroscopic fit to a separate water vapor measurement by using the measured comb repetition rate, while leaving the center frequency as a free parameter like in ref 18.

The fast rise time of the absorption (dotted frame in Figure 3) demonstrates the rapid response time of the THz DCS spectrometer. This is one of the main advantages of the dual-comb technique that differentiates it from other broadband spectroscopic techniques and allows for the study of nonrepeatable transient processes that occur on very fast time scales.[11] Figure 4a plots the absorbance of beat notes that

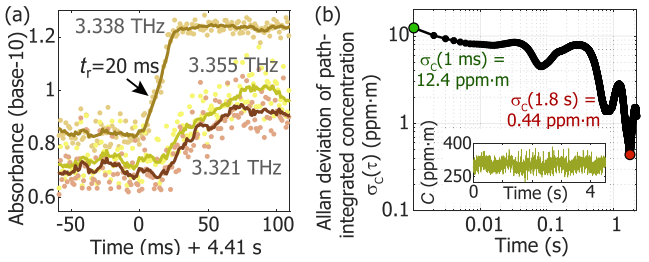

Figure 4. (a) Rapid response THz spectroscopy of water vapor. Three beat notes are strongly affected due to water vapor absorption as the measurement chamber is rapidly opened and, hence, exposed to atmospheric humidity. The 10–90% rise time (t_r) on the beat note mapping 3.338 THz is 20 ms. Solid lines are 10-point moving averages of raw data sampled every 1 ms. (b) Allan deviation of path-integrated water vapor concentration based on a HITRAN[25] database model. The curve shows a highly oscillatory shape with a global minimum at 1.8 s, corresponding to ~2 periods of cryostat vibrations. Inset shows the fitted concentrations.

map three optical frequencies: 3.338, 3.355, and 3.321 THz, of which the strongest absorption occurs at 3.338 THz. The 10–90% rise time (t_r) of the signal is 20 ms, which is not a fundamental limitation of our instrument, but rather reflects the time it takes for water vapor to diffuse into the measurement chamber. The fundamental temporal resolution limit is given by the time between consecutive DCS interferograms and is related to the rf beat note frequency spacing through $t_{min} = 1/\Delta f_{rep}$, which in our case is ~25 ns. However, this temporal resolution is accompanied by a significant reduction in signal-to-noise ratio due to random noise sources that cannot be effectively averaged. From an analogous measurement taken over 5 s, we generated an Allan deviation plot of the path-integrated water vapor concentration estimated using the HITRAN[25] database. The minimum detection limit (MDL, 1σ) reaches subppm·m after two periods of cryostat vibrations (1.8 s), while at 1 ms it reaches 12 ppm·m.

To demonstrate a spectral fitting capability, the DCS spectral data measured between 0.5–1.5 s in Figure 3 have been fitted with a HITRAN simulated mixture model containing NH_3 and residual water vapor. It should be noted that the HEB shows quadratic response with respect to optical power that is dependent on the operating temperature of the bolometer, and if not properly corrected, this nonlinearity could cause up to a factor of 2 overestimation in absorbance. Optical power management or use of Schottky mixers for dual-comb beating (ref 16) should help to mitigate these issues in the future. After the nonlinearity correction, good agreement between the spectroscopic data and the fitted model has been obtained as shown in Figure 5.

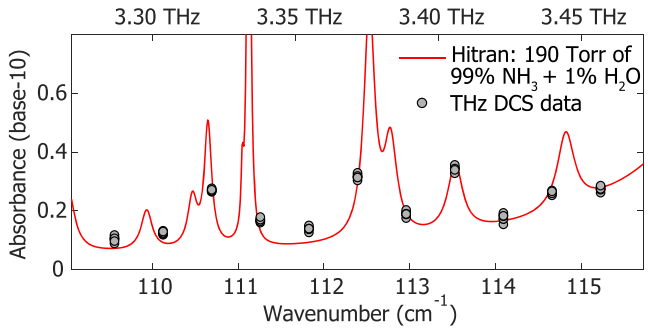

Figure 5. Fitted absorbance spectrum of 99% anhydrous NH_3 contaminated with residual amounts of water vapor measured from 0.5 to 1.5 s in 100 ms intervals.

In conclusion, we have demonstrated rapid-response QCL-based dual-comb THz measurements of gas mixtures around 3.4 THz. We probe an equilibrium reaction of NO_2/N_2O_4 as well as fast changes in concentrations of NH_3 and H_2O with a temporal resolution of 1 ms. We identify the main current limitations of the system as related to a noisy cryostat environment and bolometer nonlinearities. Other areas of improvement are the spectral resolution (~17 GHz) and the spectral coverage (~180 GHz). The former could be improved by extending the laser cavity length or by tuning the laser frequencies to fill the spectral gaps (gapless tuning).[29] The latter is constrained by the comb regime of the THz-QCL and can be addressed by future broadband QCL gain designs,[15,30] while both the ability of gap-less tuning as well as broadband operation will likely benefit from advanced dispersion compensation schemes.[14] To unlock the full potential of multispecies sensing, a multiwavelength framework[31] for estimating the pressure and concentration of individual components can also be implemented.

AUTHOR INFORMATION

Corresponding Author

Gerard Wysocki – *Department of Electrical Engineering, Princeton University, Princeton, New Jersey 08544, United States;* orcid.org/0000-0003-3727-1106; Email: gwysocki@princeton.edu

Authors

Lukasz A. Sterczewski – *Department of Electrical Engineering, Princeton University, Princeton, New Jersey 08544, United States; Laser and Fiber Electronics Group, Faculty of Electronics, Wroclaw University of Science and Technology, Wroclaw 50370, Poland*

Jonas Westberg – *Department of Electrical Engineering, Princeton University, Princeton, New Jersey 08544, United States*

Yang Yang – *Department of Electrical Engineering and Computer Science, Massachusetts Institute of Technology, Cambridge, Massachusetts 02139, United States;* orcid.org/0000-0001-5715-2206

David Burghoff – *Department of Electrical Engineering and Computer Science, Massachusetts Institute of Technology, Cambridge, Massachusetts 02139, United States; College of*

https://dx.doi.org/10.1021/acsphotonics.9b01758
ACS Photonics 2020, 7, 1082–1087

Engineering, University of Notre Dame, Notre Dame, Indiana 46556, United States

John Reno − *Center for Integrated Nanotechnology, Sandia National Laboratories, Albuquerque, New Mexico 87123, United States*

Qing Hu − *Department of Electrical Engineering and Computer Science, Massachusetts Institute of Technology, Cambridge, Massachusetts 02139, United States*

Complete contact information is available at: https://pubs.acs.org/10.1021/acsphotonics.9b01758

Author Contributions

[#]These authors contributed equally to this work.

Funding

Defense Advanced Research Projects Agency (DARPA) (W31P4Q-16-1-0001 and HR00111920006); Kosciuszko Foundation (KF; Kosciuszko Foundation Grant); Foundation for Polish Science (FNP; START 085.2018); Thorlabs Inc.; Aviation and Missile Research, Development, and Engineering Center (AMRDEC); U.S. Department of Energy (DOE); Sandia National Laboratories National Technology and Engineering Solutions of Sandia; DOE National Nuclear Security Administration (NNSA; DE-NA-0003525).

Notes

The authors declare no competing financial interest.

■ ACKNOWLEDGMENTS

The authors would like to acknowledge William H. Dix for his help with the laser submounts. The views and conclusions contained in this document are those of the authors and should not be interpreted as representing the official policies, either expressed or implied, of the DARPA, the U.S. Army, or the U.S. Government. The work in this research article was performed, in part, at the Center for Integrated Nanotechnologies, an Office of Science User Facility operated for the U.S. Department of Energy (DOE) Office of Science. Sandia National Laboratories is a multimission laboratory managed and operated by National Technology and Engineering Solutions of Sandia, LLC., a wholly owned subsidiary of Honeywell International, Inc., for the U.S. Department of Energy's National Nuclear Security Administration.

■ REFERENCES

(1) Berry, C. W.; Wang, N.; Hashemi, M. R.; Unlu, M.; Jarrahi, M. Significant performance enhancement in photoconductive terahertz optoelectronics by incorporating plasmonic contact electrodes. *Nat. Commun.* **2013**, *4*, 1622.

(2) Hu, G.; Mizuguchi, T.; Oe, R.; Nitta, K.; Zhao, X.; Minamikawa, T.; Li, T.; Zheng, Z.; Yasui, T. Dual terahertz comb spectroscopy with a single free-running fibre laser. *Sci. Rep.* **2018**, *8*, 1−9.

(3) Pagies, A.; Ducournau, G.; Lampin, J.-F. Low-threshold terahertz molecular laser optically pumped by a quantum cascade laser. *APL Photonics* **2016**, *1*, 031302.

(4) Chevalier, P.; Amirzhan, A.; Wang, F.; Piccardo, M.; Johnson, S. G.; Capasso, F.; Everitt, H. O. Widely tunable compact terahertz gas lasers. *Science* **2019**, *366*, 856−860.

(5) Faist, J.; Capasso, F.; Sivco, D. L.; Sirtori, C.; Hutchinson, A. L.; Cho, A. Y. Quantum cascade laser. *Science* **1994**, *264*, 553−556.

(6) Köhler, R.; Tredicucci, A.; Beltram, F.; Beere, H. E.; Linfield, E. H.; Davies, A. G.; Ritchie, D. A.; Iotti, R. C.; Rossi, F. Terahertz semiconductor-heterostructure laser. *Nature* **2002**, *417*, 156−159.

(7) Hübers, H.-W.; Pavlov, S.; Semenov, A.; Köhler, R.; Mahler, L.; Tredicucci, A.; Beere, H.; Ritchie, D.; Linfield, E. Terahertz quantum cascade laser as local oscillator in a heterodyne receiver. *Opt. Express* **2005**, *13*, 5890−5896.

(8) Bartalini, S.; Consolino, L.; Cancio, P.; De Natale, P.; Bartolini, P.; Taschin, A.; De Pas, M.; Beere, H.; Ritchie, D.; Vitiello, M.; et al. Frequency-comb-assisted terahertz quantum cascade laser spectroscopy. *Phys. Rev. X* **2014**, *4*, 021006.

(9) Xu, L.; Curwen, C. A.; Chen, D.; Reno, J. L.; Itoh, T.; Williams, B. S. Terahertz metasurface quantum-cascade VECSELs: Theory and performance. *IEEE J. Sel. Top. Quantum Electron.* **2017**, *23*, 1−12.

(10) Vijayraghavan, K.; Jiang, Y.; Jang, M.; Jiang, A.; Choutagunta, K.; Vizbaras, A.; Demmerle, F.; Boehm, G.; Amann, M. C.; Belkin, M. A. Broadly tunable terahertz generation in mid-infrared quantum cascade lasers. *Nat. Commun.* **2013**, *4*, 1−7.

(11) Klocke, J. L.; Mangold, M.; Allmendinger, P.; Hugi, A.; Geiser, M.; Jouy, P.; Faist, J.; Kottke, T. Single-shot sub-microsecond mid-infrared spectroscopy on protein reactions with quantum cascade laser frequency combs. *Anal. Chem.* **2018**, *90*, 10494−10500.

(12) Pinkowski, N. H.; Ding, Y.; Strand, C. L; Hanson, R. K; Horvath, R.; Geiser, M. Dual-comb spectroscopy for high-temperature reaction kinetics. *Meas. Sci. Technol.* **2020**, *31*, 055501.

(13) Villares, G.; Wolf, J.; Kazakov, D.; Süess, M. J.; Hugi, A.; Beck, M.; Faist, J. On-chip dual-comb based on quantum cascade laser frequency combs. *Appl. Phys. Lett.* **2015**, *107*, 251104.

(14) Burghoff, D.; Kao, T.-Y.; Han, N.; Chan, C. W. I.; Cai, X.; Yang, Y.; Hayton, D. J.; Gao, J.-R.; Reno, J. L.; Hu, Q. Terahertz Laser Frequency Combs. *Nat. Photonics* **2014**, *8*, 462−467.

(15) Rösch, M.; Scalari, G.; Beck, M.; Faist, J. Octave-spanning semiconductor laser. *Nat. Photonics* **2015**, *9*, 42−47.

(16) Yang, Y.; Burghoff, D.; Hayton, D. J.; Gao, J.-R.; Reno, J. L.; Hu, Q. Terahertz Multiheterodyne Spectroscopy Using Laser Frequency Combs. *Optica* **2016**, *3*, 499−502.

(17) Li, H.; Li, Z.; Wan, W.; Zhou, K.; Liao, X.; Yang, S.; Wang, C.; Cao, J.; Zeng, H. Towards Compact and Real-Time Terahertz Dual-Comb Spectroscopy Employing a Self-Detection Scheme. *ACS Photonics* **2020**, *7*, 49.

(18) Sterczewski, L. A.; Westberg, J.; Yang, Y.; Burghoff, D.; Reno, J.; Hu, Q.; Wysocki, G. Terahertz hyperspectral imaging with dual chip-scale combs. *Optica* **2019**, *6*, 766−771.

(19) Westberg, J.; Sterczewski, L.; Wysocki, G. Mid-infrared multiheterodyne spectroscopy with phase-locked quantum cascade lasers. *Appl. Phys. Lett.* **2017**, *110*, 141108.

(20) Burghoff, D.; Yang, Y.; Hu, Q. Computational Multiheterodyne Spectroscopy. *Sci. Adv.* **2016**, *2*, e1601227.

(21) Sterczewski, L. A.; Westberg, J.; Wysocki, G. Computational coherent averaging for free-running dual-comb spectroscopy. *Opt. Express* **2019**, *27*, 23875−23893.

(22) Massot, M.; Oleaga, A.; Salazar, A. Photopyroelectric Calorimetry down to 10 K. *Meas. Sci. Technol.* **2006**, *17*, 3245−3249.

(23) Caparrelli, S.; Majorana, E.; Moscatelli, V.; Pascucci, E.; Perciballi, M.; Puppo, P.; Rapagnani, P.; Ricci, F. Vibration-Free Cryostat for Low-Noise Applications of a Pulse Tube Cryocooler. *Rev. Sci. Instrum.* **2006**, *77*, 095102.

(24) Brandl, M. F.; van Mourik, M. W.; Postler, L.; Nolf, A.; Lakhmanskiy, K.; Paiva, R. R.; Möller, S.; et al. Cryogenic Setup for Trapped Ion Quantum Computing. *Rev. Sci. Instrum.* **2016**, *87*, 113103.

(25) Rothman, L. S.; Gordon, I. E.; Babikov, Y.; Barbe, A.; Benner, D. C.; Bernath, P. F.; Birk, M.; Bizzocchi, L.; Boudon, V.; Brown, L. R.; et al. The HITRAN2012 molecular spectroscopic database. *J. Quant. Spectrosc. Radiat. Transfer* **2013**, *130*, 4−50.

(26) Smith, J. O., III *Spectral Audio Signal Processing*; W3K Publishing, 2011.

(27) Givan, A.; Loewenschuss, A. Fourier transform infrared spectrum of well ordered solid dinitrogen tetroxide. *J. Chem. Phys.* **1990**, *93*, 866−867.

(28) Snyder, R. G.; Hisatsune, I. Infrared spectrum of dinitrogen tetroxide. *J. Mol. Spectrosc.* **1957**, *1*, 139−150.

(29) Gianella, M.; Nataraj, A.; Tuzson, B.; Jouy, P.; Kapsalidis, F.; Beck, M.; Mangold, M.; Hugi, A.; Faist, J.; Emmenegger, L. High-

resolution and gapless dual comb spectroscopy with current-tuned quantum cascade lasers. *Opt. Express* **2020**, *28*, 6197−6208.
(30) Yang, Y.; Paulsen, A.; Burghoff, D.; Reno, J. L.; Hu, Q. Lateral heterogeneous integration of quantum cascade lasers. *ACS Photonics* **2018**, *5*, 2742−2747.
(31) Pinkowski, N. H.; Ding, Y.; Johnson, S. E.; Wang, Y.; Parise, T. C.; Davidson, D. F.; Hanson, R. K. A multi-wavelength speciation framework for high-temperature hydrocarbon pyrolysis. *J. Quant. Spectrosc. Radiat. Transfer* **2019**, *225*, 180−205.

https://dx.doi.org/10.1021/acsphotonics.9b01758
ACS Photonics 2020, 7, 1082−1087